MODIS Multi-Angle Implementation of Atmospheric Correction (MAIAC) Data User's Guide

Collection 6 (ver. of June 2018)

Version 2.0

Principal Investigator: Alexei Lyapustin

Correspondence e-mail address:
Yujie.Wang@nasa.gov; Alexei.I.Lyapustin@nasa.gov;

Prepared by Alexei Lyapustin and Yujie Wang

Published: June 2018

TABLE OF CONTENTS

1. Introduction

MAIAC is a new advanced algorithm which uses time series analysis and a combination of pixel- and image-based processing to improve accuracy of cloud detection, aerosol retrievals and atmospheric correction (*Lyapustin et al*., 2011a,b; 2012; publication on current MAIAC is under preparation). The underlying physical idea behind MAIAC is simple: because surface changes slowly in time compared to aerosols and clouds given the daily rate of global MODIS observations, we focus on extensive characterization of the surface background in order to improve all stages of MAIAC processing. MAIAC starts with gridding MODIS measurements (L1B data) to a fixed grid at 1km resolution in order to observe the same grid cell over time and work with polar-orbiting observations as if they were "geostationary". In this regard, this approach is fundamentally different from the conventional swath-based processing where the footprint changes with orbit and view geometry (scan angle) making it difficult to characterize an always changing surface background.

To enable the time series analysis, MAIAC implements the sliding window technique by storing from 4 (at poles) to 16 (at equator) days of past observations in operational memory. This helps us retrieve surface BRDF from accumulated multi-angle set of observations, and detect seasonal (slow) and rapid surface change. A detailed knowledge of the previous surface state also helps MAIAC's internal dynamic land-water-snow classification including snow detection and characterization.

Consistently with the entire C6 MODIS land processing, the top-of-atmosphere (TOA) L1B reflectance includes standard C6 calibration (*Toller et al*., 2014) augmented with polarization correction for MODIS Terra (*Meister et al*., 2012), residual de-trending and MODIS Terra-to-Aqua cross-calibration (*Lyapustin et.al*, 2014). The L1B data are first gridded into 1km MODIS sinusoidal grid using area-weighted method (*Wolfe et al*., 1998). Due to cross-calibration, MAIAC processes MODIS Terra and Aqua jointly as a single sensor.

2. Overview of MAIAC products

MAIAC provides a suite of atmospheric and surface products in HDF4 format, including: (1) *daily* MCD19A1 (spectral BRF, or surface reflectance), (2) *daily* MCD19A2 (atmospheric properties), and (3) *8-day* MCD19A3 (spectral BRDF/albedo).

2.1 Tiled File Structure and Naming Convention

Products are generated on a 1km sinusoidal grid. The sinusoidal projection is not optimal due to distortions at high latitudes and off the grid-center, but it is a tradeoff made by the MODIS land team for the global data processing. The gridded data are divided into 1200x1200km^2 standard MODIS tiles shown in Figure 1.

The current dataset presents data per orbit (we do not provide a daily composite image as in standard MODIS surface reflectance product MOD09). Each daily file name follows the standard MODIS name convention, for instance:

MCD19A1.DayOfObservation.TileNumber.Collection.TimeOfCreation.hdf.

DayOfObservation has the format "AYYYYDDD", where YYYY is year, DDD is Julian day.

TileNumber has the standard format, e.g. h11v05 for the east coast USA.

Each daily file usually contains multiple orbit overpasses (1-2 at equator and up to 30 in polar regions for combined Terra and Aqua) which represents the third (time) dimension of MAIAC daily files. The orbit number and the overpass time of each orbit are saved in global attributes "*Orbit_amount*" and "*Orbit_time_stamp*" sequentially. The Orbit_time_stamp is in the format of "YYYYDDDHHMM[T/A]", where YYYY is year, DDD is Julian day, HH is hour MM is minute, T stands for Terra and A stands for Aqua. At high latitudes, only the first 16 orbits with largest coverage are selected for processing per day in order to limit the file size.

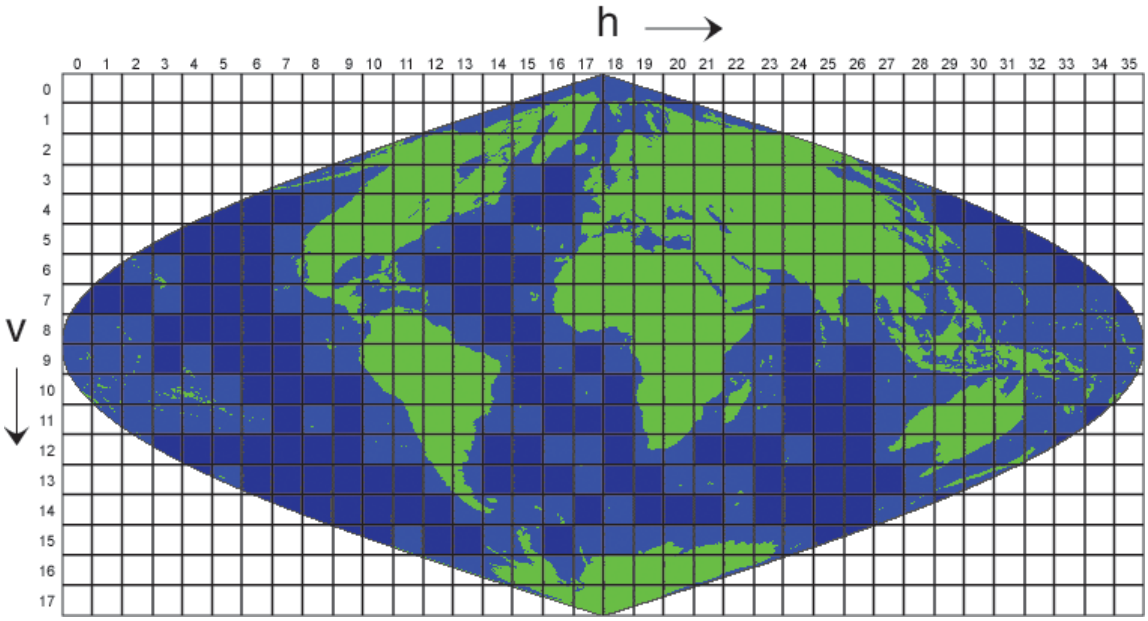

Figure 1. Illustration of MODIS Sinusoidal Tiles.

2.2 MAIAC Products: General Description

In Version 6, MAIAC spectral BRF and BRDF are considered "standard" products while aerosol optical depth (AOD) and other output fields are reported as "internal". MAIAC processing is limited to global land tiles and land-containing ocean tiles (green and light blue colors in Fig. 1).

Over inland, coastal and open ocean waters, MAIAC reports AOD, fine mode fraction, and spectral reflectance of underlight (or equivalent reflectance of water-leaving radiance).

2.2.1 Atmospheric Properties File (MCD19A2)

For each orbit, MAIAC *daily* MCD19A2 (atmospheric properties) file includes:

Over land:

- *column water vapor* (CWV) retrieved from MODIS near-IR bands B17-B19 at 0.94μm (in cm). CWV is reported for both clear and cloudy pixels. In the latter case, it represents

water vapor above the cloud;

- *aerosol optical depth and type* (background, biomass burning or dust). The AOD is originally retrieved (and reported) in MODIS Blue band B3 (0.47μm). Because the common input for the chemical transport models and GCMs as well as AOD validation and AOD product intercomparison are standardized to 0.55μm, we also provide the "Green" band (B4) AOD. It is computed from 0.47μm based on spectral properties of regional aerosol model used in retrievals. Validation shows that quality of AOD at 0.55μm is generally close though slightly worse than the original retrieval at 0.47μm. Currently, AOD is not retrieved at high altitudes >4.2km, except when Smoke/Dust aerosol is detected. Rather, we report static "climatology" value of 0.02 which is used for atmospheric correction. Our study showed that in conditions of very low AOD, non-flat terrain and generally bright surface, MAIAC aerosol retrievals at high altitudes are unreliable.
- *AOD uncertainty:* This parameter is evaluated based on the Blue-band B3 surface brightness (reflectance) only, and thus gives only a general indication of possible increase of error over brighter surfaces;
- *Injection Height* of Smoke plume (in m above ground): Reported near detected fire hot spots when smoke plume is optically thick and exhibits brightness temperature contrast with unobscured neighbor land surface. A validation against MISR MINX plume height for the North America fires of 2000-2008 showed a good accuracy within ~500m (publication in preparation).

Over water:

- *AOD* outside of glint area (glint angle ≥ 40°). When MAIAC detects dust, AOD is also reported for smaller glint angles if the retrieved value is above zero.
- *Fine Mode Fraction (FMF)* is reported along with AOD over open ocean and large in-land lakes (like Great Lakes of North America). It is not retrieved over small in-land water bodies.

View Geometry over land and water *at 5km*:

- *Cosines of Solar and View zenith angles, relative azimuth, scattering angle and glint angle*.

2.2.2 Surface Reflectance File (MCD19A1)

For each orbit, MAIAC *daily* MCD19A1 (surface reflectance) file includes:

Over land (for solar zenith angles below 80°):

- *1km BRF (surface reflectance)* in MODIS land and unsaturated ocean bands B1-B12. It is produced in cloud-free and clear-to-moderately turbid ($AOD_{0.47}$<1.5) conditions;
- *500m BRF,* nested in 1km grid, in MODIS land bands B1-B7;
- *1km BRF uncertainty (Sigma_BRFn)* in MODIS Red (B1) and NIR (B2) bands. BRF uncertainty is required for higher level land algorithms, such as LAI/FPAR (*Chen, Knyazikhin et al.*, 2017), global model assimilation, etc. We define it as a standard

deviation of the geometrically normalized BRFn over a 16-day period under the assumption that the surface is stable or changes linearly in time. As such, this is the most conservative estimate of uncertainty which includes contribution from gridding, undetected clouds, errors of atmospheric correction including those from aerosol retrievals, and of surface change when reflectance change is non-linear over time. As one can see, this definition of uncertainty is much broader than the one that may come from "theoretical" considerations, but it is also much more realistic. Sigma_BRFn in the Red band can serve as a proxy of uncertainty at shorter wavelengths, where the surface is generally darker, and the NIR value can be a proxy for the longer wavelengths with high surface reflectance.

When snow is detected, we also compute snow grain size (diameter, in mm) which governs spectral snow albedo for pure snow, and sub-pixel snow fraction. The algorithm is based on a linear mixture model of spectral snow reflectance (*Lyapustin et al.*, 2010) and pure land spectral BRDF for every land grid cell. Processing uses minimization of MODIS reflectance in bands B1, B5, B7. The residual between the best fit and MODIS observations in B1,B5,B7 is reported in parameter Snow_Fit:

- *Snow grain size* (diameter, in mm) at 1km;
- *Sub-pixel snow fraction* (range 0-1) at 1km;
- *Snow Fit* (rmse for the best fit and MODIS observations in B1,B5,B7) at 1km.

View Geometry and Kernels of RTLS BRDF model *at 5km*:

- *Cosines of Solar and View zenith angles, relative azimuth, Sun azimuth (SAZ), sensor view azimuth (VAZ), scattering angle and glint angle*.
- *Volumetric* (F_v) *and geometric-optics* (F_G) *kernels of RTLS model* for the observation geometry. Kernels are provided for geometric- (or BRDF-) normalization of spectral BRFs, which is needed in many tasks, such as change detection, geophysical and calibration trend analysis (e.g., *Lyapustin et al*., 2012; 2014) etc. Then, the BRDF (or geometry)-normalization can be done using spectral BRDF kernel weights $\{k_L, k_V, k_G\}$ from file MCD19A3 based on the following formula (see Eqs. (6) and (8) from *Lyapustin et al*., 2012):

$$BRF_n = BRF * (k_L - 0.0458621*k_V - 1.1068192*k_G)/(k_L + F_V*k_V + F_G*k_G).$$

This equation normalizes BRF from a given view geometry to the fixed geometry of nadir view and 45° solar zenith angle ($F_{0V}(45)$=-0.0458621, $F_{0G}(45)$=-1.1068192). One can easily modify normalization to a preferable Sun angle according to latitude or season, by replacing coefficients in the numerator with values from the Table 1 built for different solar zenith angles and nadir view.

The 5km reporting scale for geometry and volumetric and geometric-optics kernels is sufficient as geometry changes slowly.

SZA	F_0v(SZA)	F_{0G}(SZA)
0	0	0
1	-0.0000589	-0.0222231

2	-0.0002322	-0.0444532
3	-0.0005146	-0.0666974
4	-0.000901	-0.0889604
5	-0.0013863	-0.1112519
6	-0.0019654	-0.1335773
7	-0.0026334	-0.1559435
8	-0.0033854	-0.1783573
9	-0.0042163	-0.2008253
10	-0.0051215	-0.2233558
11	-0.006096	-0.2459545
12	-0.0071349	-0.2686286
13	-0.0082336	-0.2913864
14	-0.0093873	-0.3142342
15	-0.0105912	-0.3371795
16	-0.0118406	-0.3602294
17	-0.0131308	-0.3833919
18	-0.0144569	-0.4066738
19	-0.0158144	-0.4300835
20	-0.0171985	-0.4536282
21	-0.0186043	-0.4773155
22	-0.0200272	-0.5011534
23	-0.0214623	-0.5251498
24	-0.0229049	-0.5493125
25	-0.0243501	-0.5736493
26	-0.025793	-0.5981684
27	-0.0272287	-0.6228774
28	-0.0286523	-0.6477844
29	-0.0300587	-0.6728968
30	-0.0314429	-0.6982225
31	-0.0327997	-0.7237687
32	-0.0341241	-0.7495425
33	-0.0354105	-0.7755507
34	-0.036654	-0.8017994
35	-0.0378488	-0.8282937
36	-0.0389896	-0.8550386
37	-0.0400707	-0.8820373
38	-0.0410865	-0.9092915
39	-0.042031	-0.9368016
40	-0.0428984	-0.964565
41	-0.0436827	-0.9925762
42	-0.0443776	-1.0208257
43	-0.0449768	-1.0492985

44	-0.0454738	-1.0779734
45	-0.0458621	-1.1068192
46	-0.0461346	-1.1357927
47	-0.0462846	-1.1648338
48	-0.0463049	-1.1938568
49	-0.0461881	-1.2227401
50	-0.0459265	-1.2513024
51	-0.0455125	-1.2792587
52	-0.044938	-1.3061037
53	-0.0441948	-1.3305788
54	-0.0432743	-1.3506508
55	-0.0421677	-1.3717234
56	-0.040866	-1.3941458
57	-0.0393597	-1.4180392
58	-0.0376392	-1.44354
59	-0.0356944	-1.4708021
60	-0.033515	-1.5
61	-0.0310901	-1.5313327
62	-0.0284086	-1.5650272
63	-0.0254589	-1.6013447
64	-0.022229	-1.640586
65	-0.0187063	-1.6831008
66	-0.014878	-1.7292967
67	-0.0107305	-1.7796524
68	-0.0062498	-1.8347336
69	-0.0014212	-1.8952141
70	0.0037704	-1.9619021

Table 1. Values of V and G kernels for different SZA and nadir view (VZA=0).

2.2.3 Surface BRDF File (MCD19A3)

The *8-day* MCD19A3 (BRDF/albedo) file includes:

- *Three parameters of RTLS BRDF model* k_{iso}, k_v, k_G (here $k_{iso} = k_L$) in MODIS bands B1-B8 at *1km*. The retrievals represent cloud-free and low aerosol ($AOD_{0.47}<0.6$) conditions;
- *Spectral surface albedo* in MODIS land bands B1-B8 at 1km. It represents instantaneous albedo defined as a ratio of reflected and incident narrowband radiative fluxes at the surface. Albedo is related to BRDF retrieval and also represents cloud-free and low aerosol conditions.

Please, keep in mind that the current Terra L1B data (based on current C6 re-processed MODIS data) still contain small residual calibration artifacts which sometimes become visible as stripes in both aerosol and surface products on the right part of the scan from about middle to the edge of scan.

3. QA-related Comments (please read)

In *daily* output files, the QA bit contains cloud mask, adjacency mask, surface type (the result of MAIAC dynamic Land-Water-Snow classification), and a surface change mask.

3.1 Change in reported AOD for MAIAC AOD users:

Over land, the current C6 MAIAC AOD is reported for two values of Cloud Mask in QA bit - Clear and Possibly_Cloudy.

- Most applications should use AOD ONLY when QA.CloudMask = Clear, which guarantees high product quality.

The Possibly_Cloudy value mostly originates from spatial analysis of retrieved AOD which assumes a certain degree of aerosol spatial homogeneity (this does not apply when MAIAC detects absorbing aerosols (smoke/dust)). This filter detects residual clouds and significantly improves aerosol product quality. However:

i) The work from air quality community (Allan Just and Itai Kloog et al.) showed that in some locations with high spatial aerosol variability such as Mexico City, this filter may systematically erase AOD retrievals in cloud-free conditions over certain urban areas.

ii) This filter will also erase AOD for parts of spatially variable smoke or dust plumes where MAIAC Smoke/Dust detection failed.

For such user-specific applications (e.g., urban air quality analysis; fire smoke monitoring), we retain and report AOD when QA.CloudMask = Possibly_Cloudy.

3.2 Use of Adjacency Mask:

This mask gives information about detected neighboring clouds or snow (in the 2-pixel vicinity). For general applications, we recommend to only use data with QA.AdjacencyMask=Normal. The value 'AdjacentToASingle CloudyPixel' can also be used as it often represents false cloud detection. The other categories of 'AdjacencyMask' are not recommended when using AOD. In land analysis, we do not recommend using values 'AdjacentToCloud' and 'SurroundedByMoreThan8CloudyPixels'.

3.3 Selecting Best Quality BRF and AOD

To select best quality BRF, one should apply the following QA filter:

1. QA.AODLevel=low (0)
2. QA.AdjacencyMask=Clear
3. QA.AlgorithmInitializeStatus= initialized (0).

The best quality AOD is represented by the QA bit 0000 “Best quality”. It is a combination of the two filters:

1. QA.CloudMask = Clear
2. QA.AdjacencyMask=Clear.

4. MAIAC Data Specification

Except three reported parameters (column water vapor (cm), injection height (m above ground) and snow grain size (mm)), all other reported MAIAC products are unitless.

4.1. Surface Reflectance (MCD19A1)

SDS name	Data Type	Scale	Fill Value	Valid Range	Description
Sur_refl[1-12]	INT16	0.0001	-28672	-100 – 16000	Surface reflectance for bands 1-12
Sigma_BRFn[1-2]	INT16	0.0001	-28672	-100 – 16000	BRFn uncertainty over time, for bands 1-2
Snow_Fraction	INT16	0.0001	-28672	0 – 10000	Snow fraction (0-1)
Snow_Grain_Size	INT16	0.001	-28672	0 – 32767	Snow grain diameter (mm)
Snow_Fit	INT16	0.0001	-28672	0 – 30000	Land+Snow linear mixture model RMSE in bands 1,5,7
Status_QA	UINT16	n/a	0	1 – 65535	QA bits
Sur_refl_500m [1-7]	INT16	0.0001	-28672	-100 – 16000	Surface reflectance at 500m for band 1-7
cosSZA	INT16	0.0001	-28672	0 – 10000	Cosine of Solar zenith angle (5km)
cosVZA	INT16	0.0001	-28672	0 – 10000	Cosine View zenith angle (5km)
RelAZ	INT16	0.01	-28672	-18000 – 18000	Relative azimuth angle (5km)
Scattering_Angle	INT16	0.01	-28672	-18000 – 18000	Scattering Angle (5km)
SAZ	INT16	0.01	-28672	-18000 – 18000	Solar Azimuth Angle (5km)
VAZ	INT16	0.01	-28672	-18000 – 18000	View Azimuth Angle (5km)
Glint_Angle	INT16	0.01	-28672	-18000 – 18000	Glint Angle (5km)
Fv	FLOAT32	n/a	-99999	-100 – 100	RTLS volumetric kernel (5km)
Fg	FLOAT32	n/a	-99999	-100 - 100	RTLS geometric kernel (5km)

4.2 Status QA definition for MCD19A1 (16-bit unsigned integer)

Bits	Definition
0-2	**Cloud Mask** 000 --- Undefined 001--- Clear 010 --- Possibly Cloudy (detected by AOD filter) 011 --- Cloudy (detected by cloud mask algorithm) 101 --- Cloud Shadow 110 --- Fire hot spot (over land) 111 --- Water Sediments (over water)
3-4	**Land Water Snow/Ice Mask** 00 --- Land 01 --- Water 10--- Snow 11 --- Ice
5-7	**Adjacency Mask** 000 --- Normal condition/Clear 001 --- Adjacent to clouds 010 --- Surrounded by more than 8 cloudy pixels 011 --- Adjacent to a single cloudy pixel 100 --- Adjacent to snow 101 --- Snow was previously detected for this pixel
8	**AOD level** 0 --- AOD is low (<=0.6) 1 --- AOD is high (> 0.6) or undefined
9	**Algorithm Initialize Status** 0 --- Algorithm is initialized 1 --- Algorithm is not initialized
10	**BRF retrieved over snow assuming AOD = 0.05** 0 --- no 1 --- yes
11	**Altitude >4.2km (land)/3.5km (water), BRF is retrieved using climatology AOD =0.02** 0 --- no 1 --- yes
12-14	**Surface Change Mask** 000 --- No change 001 --- Regular change Green up 010 --- Big change Green up 011 --- Regular change Senescence 100 --- Big change Senescence **Regular Change**: Relative change in Red and NIR nadir-normalized BRF is more than 5% but less than 15% **Big Change:** Relative change in Red and NIR nadir-normalized BRF is more than 15%
15	**Reserved**

4.3 Aerosol Optical Depth (MCD19A2)

SDS name	Data Type	Scale	Fill Value	Valid Range	Description
Optical_Depth_047	INT16	0.001	-28672	-100 – 5000	Blue band aerosol optical depth
Optical_Depth_055	INT16	0.001	-28672	-100 – 5000	Green band aerosol optical depth
AOD_Uncertainty	INT16	0.0001	-28672	-100 – 30000	AOD uncertainty
FineModeFraction	INT16	0.0001	-28672	0 – 10000	Fine mode fraction for ocean
Column_WV	INT16	0.001	-28672	0 – 30000	Column Water Vapor (cm)
Injection_Height	FLOAT32	n/a	-99999	0 - 10000	Smoke injection height (m above ground)
AOD_QA	UINT16	n/a	0	1 – 65535	AOD QA
AOD_MODEL	UINT8	n/a	255	0 – 100	AOD model used in retrieval
cosSZA	INT16	0.0001	-28672	0 – 10000	Cosine of Solar zenith angle (5km)
cosVZA	INT16	0.0001	-28672	0 – 10000	Cosine of View zenith angle (5km)
RelAZ	INT16	0.01	-28672	-18000 – 18000	Relative azimuth angle (5km)
Scattering_Angle	INT16	0.01	-28672	-18000 – 18000	Scattering Angle (5km)
Glint_Angle	INT16	0.01	-28672	-18000 – 18000	Glint Angle (5km)

4.4 AOD QA definition for MCD19A2 (16-bit unsigned integer)

Bits	Definition
0-2	**Cloud Mask** 000 --- Undefined 001 --- Clear 010 --- Possibly Cloudy (detected by AOD filter) 011 --- Cloudy (detected by cloud mask algorithm) 101 --- Cloud Shadow 110 --- Hot spot of fire 111 --- Water Sediments
3-4	**Land Water Snow/ice Mask** 00 --- Land 01 --- Water 10 --- Snow 11 --- Ice
5-7	**Adjacency Mask** 000 --- Normal condition/Clear 001 --- Adjacent to clouds 010 --- Surrounded by more than 8 cloudy pixels 011 --- Adjacent to a single cloudy pixel 100 --- Adjacent to snow 101 --- Snow was previously detected in this pixel
8-11	**QA for AOD** 0000 --- Best quality 0001 --- Water Sediments are detected (water) 0011 --- There is 1 neighbor cloud 0100 --- There is >1 neighbor clouds 0101 --- No retrieval (cloudy, or whatever) 0110 --- No retrievals near detected or previously detected snow 0111 --- Climatology AOD: altitude above 3.5km (water) and 4.2km (land) 1000 --- No retrieval due to sun glint (water) 1001 --- Retrieved AOD is very low (<0.05) due to glint (water) 1010 --- AOD within +-2km from the coastline (may be unreliable) 1011 --- Land, research quality: AOD retrieved but CM is possibly cloudy
12	**Glint Mask** 0 --- No glint 1 --- Glint (glint angle < 40°)
13-14	**Aerosol Model** 00 --- Background model (regional) 01 --- Smoke model (regional) 10 --- Dust model
15	**Reserved**

4.5 8-day BRDF model parameters (MCD19A3)

SDS name	Data Type	Scale	Fill Value	Valid Range	Description
Kiso	INT16	0.0001	-32767	-32766 – 32767	RTLS isotropic kernel parameter for band 1-8
Kvol	INT16	0.0001	-32767	-32766 – 32767	RTLS volumetric kernel parameter for band 1-8
Kgeo	INT16	0.0001	-32767	-32766 – 32767	RTLS geometric kernel parameter for band 1-8
Sur_albedo	INT16	0.0001	-28672	-100 – 16000	Surface albedo for band 1-8
UpdateDay	UINT8	n/a	255	0 – 254	Number of days since last update to the current day

5. Caveats and Known Problems

1. The maximum value of LUT $AOD_{0.47}$ is 4.0 which limits characterization of strong aerosol emissions.
2. MAIAC LUTs are built assuming pseudo-spherical correction in single scattering which has a reduced accuracy for high sun/view zenith angles. A reduced MAIAC performance is expected at solar zenith angles > 70°.
3. MAIAC may be missing bright salt pans in several world deserts. In such cases, it generates a persistent high AOD resulting in missing surface retrievals.
4. Geographic AOD boundaries may sometimes be observed on borders of the regional aerosol models.
5. Because of inherent uncertainties of gridding on the coastline, the area of ±1-3 pixels from the coastline may contain frequent artifacts in cloud mask (usually over-detection), AOD (higher values) and surface BRF. Users should exercise caution near the coastline as indicated by QA.QA_AOD.
6. AC over detected snow: as MAIAC does not retrieve AOD over snow, it assumes a low climatology AOD=0.05 globally and 0.02 at high elevations (H>4.2km). Over north-central China, which is often heavily polluted and low AOD assumption can lead to a significant bias, we use AOD averaged over mesoscale area of 150km using reliable AOD retrievals over snow-free pixels. Such approach does improve quality of AC as compared to low-AOD assumption as judged by the reduced boundaries and color artefacts, but it does not account for the aerosol variability inside 150km area.
7. Ice mask is currently unreliable.
8. Consistently miss a particular type of clouds (moderately thin and homogeneous cumulus) over water generating high AOD.
9. MAIAC uses a specialized “Bay” mask for aerosol retrievals over coastal waters with high sediments. The current “Bay” mask misses at list one known area (gulf of Martaban, off the coast of Thailand) where AOD retrievals may be biased high.

We are working to resolve these issues.

6. Community Validation and Analysis of MAIAC

Since its introduction in 2011-2012, we significantly changed and improved several key parts of MAIAC, namely cloud and snow detection, characterization of spectral regression coefficient (SRC) and aerosol retrieval, and transformed the algorithm from regional to global. The intermediate versions of MAIAC were extensively tested by the land and air quality communities using our re-processing of MODIS data with the NASA Center for Climate Simulations (NCCS) and product release via NCCS ftp portal (ftp://maiac@dataportal.nccs.nasa.gov/DataRelease). Analysis by *Hilker et al*. [2012; 2014; 2015], *Maeda et al*. [2016] and others showed a dramatic (up to a factor of 3-5) increase in the accuracy of MAIAC surface reflectance compared to MODIS standard products MOD09 and MOD035 over tropical Amazon. Since 2014, all major studies of Amazon tropical forests, which used MODIS data, relied on MAIAC processing [e.g., *Saleska et al*., 2016; *Lopes et al*., 2016; *Alden et al.*, 2016; *Guan et al*., 2015; *Bi et al*., 2015, 2016; *Jones et al*., 2014; *Maeda et al*., 2017; *Wagner et al*., 2017]. Recently, *Chen et al*. [2017] reported an improvement in the leaf area index (LAI) retrievals with MODIS standard LAI/FPAR algorithm based on MAIAC instead of MOD09 input. A good accuracy, high 1km spatial resolution and high retrieval coverage made MAIAC aerosol optical depth (AOD) a focus of numerous air quality studies, e.g. [*Chudnovsky et al*., 2013; *Kloog et al*., 2014; *Just et al.*, 2015; *Di et al.*, 2016; *Tang et al*., 2017; *Xiao et al*., 2017] just to name a few. Currently published validation studies [*Martins et al*., 2017; *Superczynski et al*, 2017] show a good MAIAC AOD accuracy over American continents, and a significantly better accuracy and coverage over North America than the operational VIIRS algorithm [*Superczynski et al*, 2017]. An emerging comparative aerosol validation analysis over North America [*Jethva et al., to be submitted*] and South Asia [*Mhawish et al., in review*] shows that MAIAC has a comparable or improved accuracy to the Dark Target [*Levy et al*., 2013] algorithm over dark surfaces and generally improves accuracy over the Deep Blue (DB) algorithm [*Hsu et al*., 2013] over bright surfaces.

At this stage, most accuracy assessments of the standard MODIS algorithms can be applied to MAIAC products. For instance, MAIAC AOD accuracy can be evaluated as ±0.05 ±0.15AOD.

According to the MODIS land team guidelines (https://landweb.modaps.eosdis.nasa.gov/cgi-bin/QA_WWW/newPage.cgi?fileName=maturity), the current MAIAC validation status can be characterized as follows:

- Atmospheric Products (MCD19A2):
  - AOD: Stage 3;
  - Column Water Vapor: between stage 2 and 3 (globally validated for 2000-2005; validation for South America for 2000-2015);
  - Aerosol Plume Height: Stage 1;
- Land Surface Reflectance Suite (MCD19A1): Stage 1;
- BRDF/Albedo (MCD19A3): Stage 1.

7. Data ordering (browsing)

7.1. Data Access

The following tools offer options to search the LP DAAC (**(Land Processes Distributed Active Archive Center)** data holdings and provide access to the data:

1) Bulk download: LP DAAC Data Pool (https://lpdaac.usgs.gov/data_access/data_pool) and DAAC2Disk (https://lpdaac.usgs.gov/data_access/daac2disk)
2) Search and browse: USGS EarthExplorer (https://earthexplorer.usgs.gov/) and NASA Earthdata Search (https://search.earthdata.nasa.gov/search)
3) MODIS Land Global Browse Images
   5-km versions of selected product to enable synoptic quality assessment.
   Link: http://landweb.nascom.nasa.gov/cgi-bin/browse/browse.cgi

Note: USGS EarthExplorer access to the data will follow soon after public release.

REFERENCES

Alden, C. B. et al., (2016), Regional atmospheric CO2 inversion reveals seasonal and geographic differences in Amazon net biome exchange. *Glob Change Biol.* doi:10.1111/gcb.13305.

Bi J, Knyazikhin Y, Choi S, Park T, Barichivich J, Ciais P, Fu R, Ganguly S, Hall F, Hilker T, Huete A, Jones M, Kimball J, Lyapustin A, Mottus M, Nemani R, Piao S, Poulter B, Saleska S, Saatchi S, Xu L, Zhou L, Myneni R., Sunlight mediated seasonality in canopy structure and photosynthetic activity of Amazonian rainforests, *Environ. Res. Lett*., 10(6):6, 2015, 10.1088/1748-9326/10/6/064014.

Bi, J., R. Myneni, A. Lyapustin, Y. Wang, T. Park, C. Chen, K. Yan, Y. Knyazikhin, Amazon forests' response to droughts: a perspective from the MAIAC product, *Remote Sens*., 2016, 8, 356; doi:10.3390/rs8040356.

Chen, C., Y. Knyazikhin, T. Park, K. Yan, A. Lyapustin, Y. Wang, B. Yang and R. B. Myneni, Prototyping of LAI and FPAR Algorithm with MODIS MultiAngle Implementation of Atmospheric Correction (MAIAC) data, *Rem. Sensing*, 2017, 9, 370; doi:10.3390/rs9040370.

Chudnovsky, A., Tang, C., Lyapustin, A., Wang, Y., Schwartz, J., and Koutrakis, P., 2013: A Critical Assessment of High Resolution Aerosol Optical Depth (AOD) Retrievals for fine particulate matter (PM) Predictions, *Atmos. Chem. Phys*., 13, 10907-10917, https://doi.org/10.5194/acp-13-10907-2013, 2013.

Di, Qian, I. Kloog, P. Koutrakis, A. Lyapustin, Y. Wang and J. Schwartz, Assessing PM2.5 Exposures with High Spatiotemporal Resolution across the Continental United States, *Environmental science & technology*, 50 9 (2016): 4712-21, **doi:** 10.1021/acs.est.5b06121.

Guan, K., Pan, M., Li, H., Wolf, A., Wu, J., Medvigy, D., Caylor, K. K., Sheffield J., Wood, E.F., Malhi, Y., Liang, M., Kimball, J. S., Saleska, S., Berry, J., Joiner, J., and Lyapustin, A. I. (2015) "Photosynthetic seasonality of global tropical forests constrained by hydroclimate", *Nature Geoscience*, 8, 284-289, doi: 10.1038/NGEO2382.

Hilker, T., A. Lyapustin, F. G. Hall, Y. Wang, N. C. Coops, G. Drolet, & T. A. Black, 2009: An assessment of photosynthetic light use efficiency from space: Modeling the atmospheric and directional impacts on PRI reflectance. *Rem. Sens. Environment*, **113**, 2463-2475.

Hilker, T., Hall, F., Coops, N.C., Lyapustin, A., Wang, Y., Nesic, Z., Grant, N., Black, T.A. Wulder, MA., Kljun, N., Hopkinson, C., Chaser, L., 2010: Remote sensing of photosynthetic light-use efficiency across two forested biomes: Spatial scaling. *Rem. Sens. Environ*., 114, 2863-2874.

Hilker, T., A. I. Lyapustin, C. J. Tucker, P. J. Sellers, F. G. Hall, Y. Wang, 2012: Remote Sensing of Tropical Ecosystems: Atmospheric Correction and Cloud Masking Matter. *Rem. Sens. Environ.*, http://dx.doi.org/10.1016/j.rse.2012.08.035**.**

Hilker, T., A. I. Lyapustin, C. J. Tucker, F. G. Hall, R. B. Myneni, Y. Wang, J. Bi, Y. M. de Moura, P. J. Sellers (2014), Vegetation dynamics and rainfall sensitivity of the Amazon, *PNAS*, 111 (45), 16041-16046, doi:10.1073/pnas.1404870111.

Hilker, T., A. I. Lyapustin, Y. Wang, F. G. Hall, C. J. Tucker, P. J. Sellers, On the measurability of change in Amazon vegetation from MODIS, *Remote Sens. Environ*., 166, 233-242, 2015.

Hsu, N.-Y. C., M.-J. Jeong, C. Bettenhausen, et al. A. M. Sayer, R. A. Hansell, C. S. Seftor, J. Huang, and S.-C. Tsay. 2013. "Enhanced Deep Blue aerosol retrieval algorithm: The second generation." *J. Geophys. Res. Atmos*., 118 (16)**:** 9296–9315 [10.1002/jgrd.50712.

Hu, X., L. A. Waller, A. Lyapustin, Y. Wang, M.Z. Al-Hamdan, W.L. Crosson, M.G. Estes Jr., S.M. Estes, D.A. Quattrochi, S.J. Puttaswamy, and Y. Liu, 2014: Estimating Ground-Level PM2.5 Concentrations in the Southeastern United States Using MAIAC AOD Retrievals and a Two-Stage Model, *Rem. Sens. Environ*, *140, 220-232*.

Jackson, J. M., H. Liu, I. Laszlo, S. Kondragunta, L. A. Remer, J. Huang, and H. C. Huang (2013), Suomi-NPP VIIRS aerosol algorithms and data products, *J. Geophys. Res. Atmos*., 118, 12–673, doi:10.1002/2013JD020449.

Jones, M. O., Kimball J. S., and Nemani R. R., Asynchronous Amazon forest canopy phenology indicates adaptation to both water and light availability, *Environ. Res. Letters*, 9, 1-10, 2014, doi: 10.1088/1748-9326/9/12/124021.

Just A, Wright R, Schwartz J, Coull B, Baccarelli A, Maria Tellez-Rojo M, Moody E, Wang Y, Lyapustin A, Kloog I. Using High-Resolution Satellite Aerosol Optical Depth To Estimate Daily PM2.5 Geographical Distribution in Mexico City, *Environ. Sci. Technol.*, 49 (14):8576-8584, 2015, 10.1021/acs.est.5b00859.

Kloog, I., A. A. Chudnovsky, A. C. Just, F. Nordio, P. Koutrakis, B. A. Coull, A. I. Lyapustin, Y. Wang, and J. Schwartz. 2014. "A new hybrid spatio-temporal model for estimating daily multi-year PM2.5 concentrations across northeastern USA using high resolution aerosol optical depth data." *Atmos. Environ*., 95, 581–590, doi:10.1016/j.atmosenv.2014.07.014.

Levy, R. C., Mattoo, S., Munchak, L. A., Remer, L. A., Sayer, A. M., Patadia, F., and Hsu, N. C.: The Collection 6 MODIS aerosol products over land and ocean, *Atmos. Meas. Tech*., 6, 2989–3034, doi:10.5194/amt-6-2989-2013, 2013.

Lopes, A.P., et al. (2016), Leaf flush drives dry season green-up of the Central Amazon, *Rem. Sens. Environ.*, 182, 90–98.

Lyapustin, A., Y. Wang, S. Korkin, MODIS Collection 6 MAIAC Algorithm, *Atmos. Meas. Tech.*, in review.

Lyapustin, A., C. K. Gatebe, R. Kahn, R. Brandt, J. Redemann, P. Russell, M. D. King, C. A. Pedersen, S. Gerland, R. Poudyal, A. Marshak, Y. Wang, C. Schaaf, D. Hall, and A. Kokhanovsky, 2010: Analysis of Snow Bidirectional Reflectance from ARCTAS Spring-2008 Campaign. *Atmos. Chem. Phys.*, **10**, 4359-4375.

Lyapustin, A., J. Martonchik, Y. Wang, I. Laszlo, S. Korkin, 2011a: Multi-Angle Implementation of Atmospheric Correction (MAIAC): Part 1. Radiative Transfer Basis and Look-Up Tables, *J. Geophys. Res*., 116, D03210, doi:10.1029/2010JD014985.

Lyapustin, A., Y. Wang, I. Laszlo, R. Kahn, S. Korkin, L. Remer, R. Levy, and J. S. Reid, 2011b: Multi-Angle Implementation of Atmospheric Correction (MAIAC): Part 2. Aerosol Algorithm, *J. Geophys. Res*., 116, D03211, doi:10.1029/2010JD014986.

Lyapustin, A., Y. Wang, I. Laszlo, T. Hilker, F. Hall, P. Sellers, J. Tucker, S. Korkin, 2012: Multi-Angle Implementation of Atmospheric Correction for MODIS (MAIAC). 3: Atmospheric Correction. *Rem. Sens. Environ*. (2012), http://dx.doi.org/10.1016/j.rse.2012.09.002.

Lyapustin, A., Y. Wang, X. Xiong, G. Meister, S. Platnick, R. Levy, B. Franz, S. Korkin, T. Hilker, J. Tucker, F. Hall, P. Sellers, A. Wu, A. Angal (2014), Science Impact of MODIS C5 Calibration Degradation and C6+ Improvements, *Atmos. Meas. Tech.*, 7, 4353-4365, doi:10.5194/amt-7-4353-2014.

Maeda, E.E., Mendes Moura, Y., Wagner,F., Hilker, T., Lyapustin, A.I., Wang, Y., Mõttus,M., Aragão, L.E.O.C., Shimabukuro Y. Consistency of vegetation index seasonality across the Amazon rainforest. *Int.J. Appl. Earth Observation & Geoinformation*, *52*, 42-53, 2016.

Maeda, E.E., et al., Evapotranspiration seasonality across the Amazon basin, *Earth Syst. Dynam. Discuss*., doi:10.5194/esd-2016-75, 2017.

Martins, V. S., A. Lyapustin, L. A. S. de Carvalho, C. C. F. Barbosa, and E. M. L. M. Novo (2017), Validation of high-resolution MAIAC aerosol product over South America, *J. Geophys. Res. Atmos*., 122, doi:10.1002/2016JD026301.

Meister, G., B. Franz, E. Kwiatkowska, and C. McClain (2012). Corrections to the Calibration of MODIS Aqua Ocean Color Bands derived from SeaWiFS Data, *IEEE TGARS*, *50*(1), 310 – 319, doi: 10.1109/TGRS.2011.2160552.

Saleska, S. R., Wu, J., Guan, K., Restrepo-Coupe, N., Nobre, A. D., Araujo, A., & Huete, A. R. (2016). Dry-season greening of Amazon forests. *Nature Brief Communication Arising*, 531(7594), E4–E5. http://dx.doi.org/10.1038/nature16457.

de Sousa C., T. Hilker, R. Waring, Y. de Moura, A. Lyapustin, Progress in Remote Sensing of Photosynthetic Activity over the Amazon Basin, *Remote Sens.* **2017**, *9*(1), 48; doi:10.3390/rs9010048.

Stafoggia, M., J. Schwartz, C. Badaloni, T. Bellander, E. Alessandrini, G. Cattani, F. de' Donato, A. Gaeta, G. Leone, A. Lyapustin, M. Sorek-Hamer, K. de Hoogh, Q. Di, F. Forastiere, I. Kloog, Estimation of daily PM10 concentrations in Italy (2006–2012) using finely resolved satellite data, land use variables and meteorology, *Environ. Int.* (2016), http://dx.doi.org/10.1016/j.envint.2016.11.024.

Superczynski S., S. Kondragunta, A. Lyapustin. Evaluiation of the Multi-Angle Implementation of Atmospheric Correction (MAIAC) Aerosol Algorithm through Intercomparison with VIIRS Aerosol Products and AERONET, *J. Geophys. Res.-Atmos*., 2017, 122, 3005-3022, doi:10.1002/2016JD025720.

Toller, G., X. Xiong, J. Sun, B. N. Wenny, X. Geng, J. Kuyper, A. Angal, H. Chen, S. Madhavan, and A. Wu, "Terra and Aqua Moderate-resolution Imaging Spectroradiometer Collection 6 Level 1B Algorithm", J. Applied Remote Sensing, 7(1), 2013, 0001;7(1):073557-073557. doi:10.1117/1.JRS.7.073557.

Vermote, E. F.**,** and Kotchenova, S., 2008: Atmospheric correction for the monitoring of land surfaces. *J. Geophys. Res.*, 113, D23S90, doi:10.1029/2007JD009662.

Wagner, F.H., B. Herault, V. Rossi, T. Hilker, E.E. Maeda, A. Sanchez, A.I. Lyapustin, L.S. Galvao, Y. Wang, L.E.O.C. Aragao, Climate drivers of the Amazon forest greening, *Public Library of Science (PLOS ONE*), July 2017.

Wolfe, R. E., Roy, D. P., and Vermote (1998). E. MODIS Land Data Storage, Gridding, and Compositing Methodology: Level 2 Grid. *IEEE Trans. Geosci. Remote Sens.*, *36*, 1324–1338.

Xiao, Q., Y. Wang, H.H. Chang, X. Meng, G. Geng, A. Lyapustin, Y. Liu, Full-coverage high-resolution daily $PM_{2.5}$ estimation using MAIAC AOD in the Yangtze River Delta of China, *Rem. Sens. Environ*., 2017 http://dx.doi.org/10.1016/j.rse.2017.07.023.

We are looking forward to your comments, suggestions, etc. which you may forward either to myself (Alexei.I.Lyapustin@nasa.gov) or to Yujie (Yujie.Wang@nasa.gov).

We acknowledge the support from MODAPS and MODIS LAADS in accommodating processing and data archive.